Stability of systems with state delay subjected to digital control

David Lehotzky and Tamas Insperger

Abstract Stability of linear delayed systems subjected to digital control is analyzed. These systems can typically be written in the form

$$\dot{\mathbf{x}}(t) = \mathbf{A}\mathbf{x}(t) + \mathbf{B}\mathbf{x}(t-\tau) + \mathbf{C}\mathbf{x}(t_{j-1}) \ , \quad t \in [t_j, t_{j+1}) \ ,$$

where $t_j = j\Delta t$ with Δt being the sampling period for the digital controller. The point-delay term $\mathbf{x}(t-\tau)$ is assumed to be inherently present in the governing equation of the uncontrolled system, while the term $\mathbf{x}(t_{j-1})$ is present due to the digital controller. Since the term $\mathbf{x}(t_{j-1})$ can be represented as a term with a piecewise linearly varying time delay, the system is time-periodic at period Δt. The stability analysis for the system is performed using the semi-discretization method. As case studies, the stability charts of the delayed oscillator and the turning process are determined for a digital PD controller.

1 Introduction

Time delays are often inherently present in mechanical systems due to physical interactions between different elements of the system or due to a feedback mechanism. For instance, in wheel shimmy models, the contact between elastic tires and the road is described by a delay-differential equation (DDE) with distributed delay [29]. In car following traffic models, time delay arise due to the reflex delay of the drivers [17]. Machine tool chatter is also modeled by DDEs, where the delay

---

David Lehotzky
Budapest University of Technology and Economics, Department of Applied Mechanics, Budapest, Hungary e-mail: `lehotzkydavid@gmail.com`

Tamas Insperger
Budapest University of Technology and Economics, Department of Applied Mechanics, Budapest, Hungary e-mail: `insperger@mm.bme.hu`

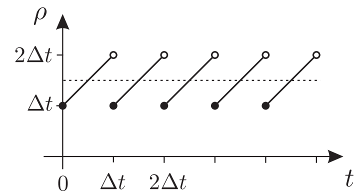

Fig. 1 Representation of the sampling effect as time-varying delay

appears due to the regenerative effect as result of the contact of the tool and the workpiece. For simple tool geometry, the regenerative delay can be modeled by a point delay [1], while for more complex tool geometry, such as a milling tool with varying helix angle, the surface regeneration can be described by a distributed delay [4]. In these examples, time delays inherently arise due to the structure of the mechanical system and the delayed terms in the governing equations are continuous in time. If these systems are subjected to a digital feedback controller, then discrete-delay terms (i.e., terms with piecewise constant argument) also arise due to the sampling effect [18, 24]. The goal of this chapter is to analyze the stability of systems, where both continuous- and discrete-time delayed terms appears.

Here, we consider Newtonian systems with point delay in the position term subjected to a digital proportional-derivative (PD) controller. The governing equation of such systems can be given in the form

$$\mathbf{M}\ddot{\mathbf{q}}(t)+\mathbf{C}\dot{\mathbf{q}}(t)+\mathbf{K}\mathbf{q}(t) = \mathbf{H}\mathbf{q}(t-\tau)+\mathbf{K}_{\mathrm{p}}\mathbf{q}(t_{j-1})+\mathbf{K}_{\mathrm{d}}\dot{\mathbf{q}}(t_{j-1}) \ , \quad t \in [t_j, t_{j+1}) \ , \tag{1}$$

where $\mathbf{q} \in \mathbb{R}^n$ is the vector of the general coordinates, $\mathbf{M}$, $\mathbf{C}$ and $\mathbf{K}$ are the mass, the damping and the stiffness matrices, $\mathbf{H}$ is a matrix describing the delay effect, τ is the system delay, $\mathbf{K}_{\mathrm{p}}$ and $\mathbf{K}_{\mathrm{d}}$ are the proportional and derivative control matrices, Δt is the sampling step of the digital controller and $t_j = j\Delta t$ are the discrete sampling instants. Thus, the system contains two types of delay terms, the continuous-time point-delay term $\mathbf{q}(t-\tau)$ and the discrete-time delay terms $\mathbf{q}(t_{j-1})$ and $\dot{\mathbf{q}}(t_{j-1})$ with piecewise constant argument over the sampling interval $[t_j, t_{j+1})$. Actually, the terms $\mathbf{q}(t_{j-1})$ and $\dot{\mathbf{q}}(t_{j-1})$ can be represented as terms with periodic time delay in the form $\mathbf{q}(t-\rho(t))$ and $\dot{\mathbf{q}}(t-\rho(t))$, where the time delay is a piecewise linear function given as $\rho(t) = t + \Delta t - t_j$, $t \in [t_j, t_{j+1})$ (see Fig. 1). According to this interpretation, sampling in the feedback loop presents a parametric excitation in the time delay and the period of the parametric excitation is equal to the sampling period Δt. Consequently, the governing equation is a periodic DDE, and the stability analysis can be performed according to the Floquet theory of DDEs [5, 7]. There exists several numerical methods for the stability analysis of periodic DDEs, the semi-discretization [9, 10], the Chebyshev polynomial approach [2], the spectral element method [11], the method of characteristic matrices [22, 28], Hill's method [12], the full-discretization method [3,19] or the continuous time approximation [25, 26] can be mentioned as examples. In this chapter, the stability analysis of equation

(1) is presented using the semi-discretization method according to [9, 10]. As a new concept, one- and two-points methods with different order of approximations are introduced in the discretization scheme.

2 Semi-Discretization

The first-order representation of equation (1) reads

$$\dot{\mathbf{x}}(t) = \mathbf{A}\mathbf{x}(t) + \mathbf{B}\mathbf{x}(t-\tau) + \mathbf{C}\mathbf{x}(t_{j-1}) \ , \quad t \in [t_j, t_{j+1}) \ , \tag{2}$$

where

$$\mathbf{x}(t) = \begin{pmatrix} \mathbf{q}(t) \\ \dot{\mathbf{q}}(t) \end{pmatrix} , \ \mathbf{A} = \begin{pmatrix} \mathbf{0} & \mathbf{I} \\ -\mathbf{M}^{-1}\mathbf{K} & -\mathbf{M}^{-1}\mathbf{C} \end{pmatrix} , \ \mathbf{B} = \begin{pmatrix} \mathbf{0} & \mathbf{0} \\ \mathbf{H} & \mathbf{0} \end{pmatrix} , \ \mathbf{C} = \begin{pmatrix} \mathbf{0} & \mathbf{0} \\ \mathbf{K}_{\mathrm{p}} & \mathbf{K}_{\mathrm{d}} \end{pmatrix} . \tag{3}$$

Semi-discretization is a numerical technique which can be used for the stability analysis of time-periodic DDEs [9, 10]. The method gives a finite dimensional approximation for the infinite dimensional eigenvalue problem of time-delayed systems. The description presented here is valid for the case when the system delay τ is integer multiple of the sampling period $\varDelta t$, i.e., when $\kappa = \tau/\varDelta t \in \mathbb{Z}$. The semi-discretization is based on the discrete time scale $t_i = ih$, where h is the discretization step determined as $\tau = rh$ and $\varDelta t = ph$. Here, r is the delay resolution, p is the period resolution. Clearly, $r/p = \tau/\varDelta t = \kappa$. Note that subscript i is used for the discrete time scale of the semi-discretization, while subscript j is used for the discrete time scale $t_j = j\varDelta t$ due to the sampling of the controller. In the next two subsections, two types of discretization schemes, the one-point method and the two-point method are detailed.

2.1 One-point methods

One-point methods approximate the delayed value of the state variables with values taken from one discrete past time instant. The approximation of equation (1) for the time interval $t \in [t_i, t_{i+1})$ can be given as

$$\dot{\mathbf{x}}(t) = \mathbf{A}\mathbf{x}(t) + \mathbf{D}(t)\mathbf{x}_{i-r} + \mathbf{C}\mathbf{x}_{i-p} \ , \tag{4}$$

where $\mathbf{D}(t)$ is a weighting matrix which depends on the method and the order of the approximation. Short hand notation is used for $\mathbf{x}(t_{i-r}) = \mathbf{x}_{i-r}$ and respectively for the similar terms. The sketch of the semi-discretization for the case of the zeroth-order one-point method for different steps is shown in Fig. 2 for $r = 20$, $p = 5$ and, consequently, $\kappa = 4$. The initial condition for equation (4) is $\mathbf{x}(t_i) = \mathbf{x}_i$, which provides the continuity of the displacement and velocity functions at time instant

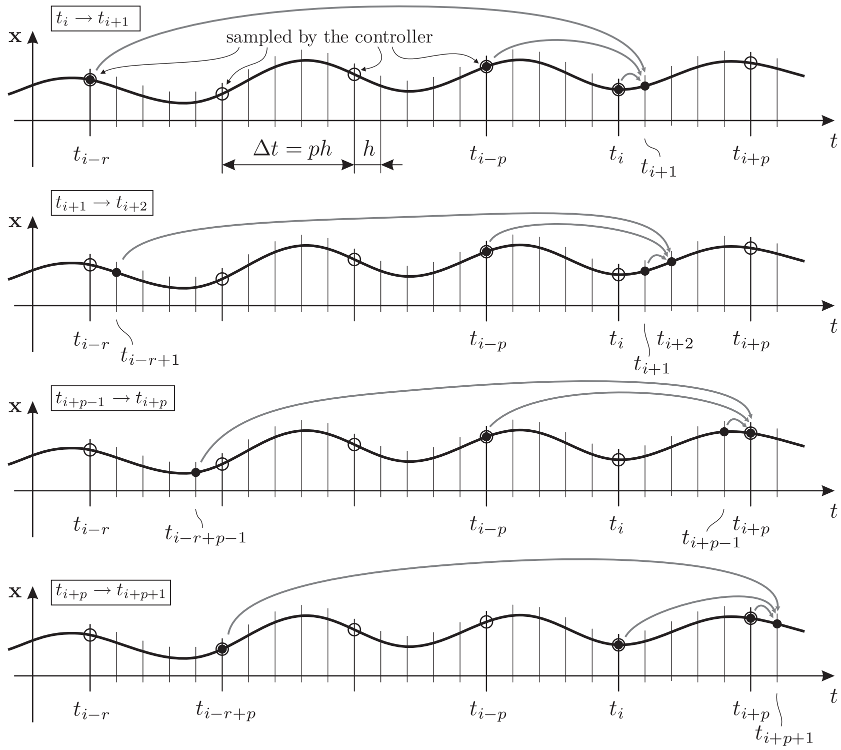

Fig. 2 Sketch of the discretization for the case of zeroth-order one-point method at different steps

$t = t_i$. Using the variation of constants formula, the solution for (4) can be given as

$$\mathbf{x}(t) = \mathbf{e}^{\mathbf{A}(t-t_i)}\mathbf{x}_i + \int_0^{t-t_i} \mathbf{e}^{\mathbf{A}(t-t_i-s)} \left(\mathbf{D}(s)\mathbf{x}_{i-r} + \mathbf{C}\mathbf{x}_{i-p}\right) \mathrm{d}s. \tag{5}$$

Hence the relation between the two end points of the discretization interval is

$$\mathbf{x}_{i+1} = \mathbf{P}\mathbf{x}_i + \mathbf{R}_1\mathbf{x}_{i-r} + \mathbf{R}_C\mathbf{x}_{i-p}, \tag{6}$$

where

$$\mathbf{P} = \mathbf{e}^{\mathbf{A}h}\ , \quad \mathbf{R}_1 = \int_0^h \mathbf{e}^{\mathbf{A}(h-t)}\mathbf{D}(t)\mathrm{d}t\ , \quad \mathbf{R}_C = \int_0^h \mathbf{e}^{\mathbf{A}(h-t)}\mathbf{C}\mathrm{d}t\ . \tag{7}$$

If $\mathbf{A}^{-1}$ exist, then

$$\mathbf{R}_C = -\mathbf{A}^{-1}\left(\mathbf{I} - \mathrm{e}^{\mathbf{A}h}\right)\mathbf{C}\ , \tag{8}$$

where $\mathbf{I}$ denotes the unit matrix. Equation (6) implies the discrete map

$$\mathbf{X}_{i+1} = \mathbf{G}_1 \mathbf{X}_i \ , \tag{9}$$

where

$$\mathbf{X}_i = \begin{pmatrix} \mathbf{x}_i \ \mathbf{x}_{i-1} \ \ldots \ \mathbf{x}_{i-r} \end{pmatrix}^T \tag{10}$$

is an augmented state vector, and the coefficient matrix for this first step reads

$$\mathbf{G}_1 = \begin{pmatrix} \mathbf{P} & \mathbf{0} & \ldots & \mathbf{0} & \mathbf{R}_C & \mathbf{0} & \mathbf{0} & \ldots & \mathbf{0} & \mathbf{0} & \mathbf{R}_1 \\ \mathbf{I} & \mathbf{0} & \ldots & \mathbf{0} & \mathbf{0} & \mathbf{0} & \mathbf{0} & \ldots & \mathbf{0} & \mathbf{0} & \mathbf{0} \\ \mathbf{0} & \mathbf{I} & & \mathbf{0} & \mathbf{0} & \mathbf{0} & \mathbf{0} & & \mathbf{0} & \mathbf{0} & \mathbf{0} \\ \vdots & & & & & & & & & & \vdots \\ \mathbf{0} & \mathbf{0} & & \mathbf{0} & \mathbf{0} & \mathbf{0} & \mathbf{0} & & \mathbf{I} & \mathbf{0} & \mathbf{0} \\ \mathbf{0} & \mathbf{0} & \ldots & \mathbf{0} & \mathbf{0} & \mathbf{0} & \mathbf{0} & \ldots & \mathbf{0} & \mathbf{I} & \mathbf{0} \end{pmatrix} . \tag{11}$$

Note that this matrix consists of submatrices of size $2n \times 2n$, namely, $\mathbf{P}$, $\mathbf{R}_C$, $\mathbf{R}_1$, the $2n \times 2n$ unit matrix $\mathbf{I}$ and the $2n \times 2n$ zero matrix $\mathbf{0}$. Matrix $\mathbf{R}_C$ is located at the $(p+1)$th block in the first row of $\mathbf{G}_1$.

Since the control force is constant over the sampling period $[t_i, t_{i+p})$, the approximate differential equation for the second discretization step is

$$\dot{\mathbf{x}}(t) = \mathbf{A}\mathbf{x}(t) + \mathbf{D}(t)\mathbf{x}_{i-r+1} + \mathbf{C}\mathbf{x}_{i-p} \ , \quad t \in [t_{i+1}, t_{i+2}) \ . \tag{12}$$

Solving this differential equation similarly to (4), the difference equation between the endpoints of the second discretization is obtained in the form

$$\mathbf{X}_{i+2} = \mathbf{G}_2 \mathbf{X}_{i+1} \ , \tag{13}$$

where the state vector is $\mathbf{X}_i$ is defined as in (10), and the coefficient matrix for the second step reads

$$\mathbf{G}_2 = \begin{pmatrix} \mathbf{P} & \mathbf{0} & \ldots & \mathbf{0} & \mathbf{0} & \mathbf{R}_C & \mathbf{0} & \ldots & \mathbf{0} & \mathbf{0} & \mathbf{R}_1 \\ \mathbf{I} & \mathbf{0} & \ldots & \mathbf{0} & \mathbf{0} & \mathbf{0} & \mathbf{0} & \ldots & \mathbf{0} & \mathbf{0} & \mathbf{0} \\ \mathbf{0} & \mathbf{I} & & \mathbf{0} & \mathbf{0} & \mathbf{0} & \mathbf{0} & & \mathbf{0} & \mathbf{0} & \mathbf{0} \\ \vdots & & & & & & & & & & \vdots \\ \mathbf{0} & \mathbf{0} & & \mathbf{0} & \mathbf{0} & \mathbf{0} & \mathbf{0} & & \mathbf{I} & \mathbf{0} & \mathbf{0} \\ \mathbf{0} & \mathbf{0} & \ldots & \mathbf{0} & \mathbf{0} & \mathbf{0} & \mathbf{0} & \ldots & \mathbf{0} & \mathbf{I} & \mathbf{0} \end{pmatrix} . \tag{14}$$

Here, matrix $\mathbf{R}_C$ is located at the $(p+2)$th block in the first row of $\mathbf{G}_2$. The only difference between matrices $\mathbf{G}_1$ and $\mathbf{G}_2$ is the location of the sub-matrix $\mathbf{R}_C$. While in $\mathbf{G}_1$, $\mathbf{R}_C$ is located at the $(p+1)$th block in the first row, in $\mathbf{G}_2$, matrix $\mathbf{R}_C$ is located at the $(p+2)$th block in the first row.

For the next discretization interval $[t_{i+2}, t_{i+3})$, matrix $\mathbf{R}_C$ is located at the $(p+3)$th block in the first row, etc. With the induction of this phenomena the structure of the first row of $\mathbf{G}$ is shown in Fig. 3 for different discretization steps.

For the stability analysis of the approximate system (4), the solution should be determined over the period $\Delta t = ph$ of the parametric excitation (i.e., over the

$$\begin{bmatrix} \overbrace{\mathbf{P}\;\mathbf{0}\;\dots\;\mathbf{0}}^{p} & \overbrace{\mathbf{R}_C \overset{2}{\curvearrowright} \mathbf{0} \overset{3}{\curvearrowright} \dots \overset{p-1}{\curvearrowright} \mathbf{0} \overset{p}{\curvearrowright} \mathbf{0}}^{p} & \overbrace{\mathbf{0}\;\dots\;\mathbf{0}\;\mathbf{R}_1}^{r-2p+1} \end{bmatrix}$$

Fig. 3 Top row of $\mathbf{G}$ matrices for one-point methods

principal period). The monodromy mapping for the initial state $\mathbf{X}_i$ is given as

$$\mathbf{X}_{i+p} = \mathbf{\Phi}\mathbf{X}_i, \tag{15}$$

where $\mathbf{\Phi} = \mathbf{G}_p\,\mathbf{G}_{p-1}\dots\mathbf{G}_2\,\mathbf{G}_1$ is the monodromy matrix (Floquet transition matrix). The condition for asymptotic stability is that all eigenvalues of $\mathbf{\Phi}$ must be in modulus less then 1, formally

$$|\mu_{\text{max}}| < 1\ , \tag{16}$$

where $\mu_{\text{max}} = \max(\mu_i)$ with μ_i, $i = 1, 2, \dots, (n+1)r$ being the eigenvalues of $\mathbf{\Phi}$.

As it was mentioned earlier, semi-discretization of different orders can be represented by the weighting matrix $\mathbf{D}(t)$. In the next points, the zeroth-order and the first-order approximations will be presented for the one-point method.

2.1.1 Zeroth-order approximation

This method uses only the discrete vector $\mathbf{q}(t_{i-r})$ of general coordinates to approximate $\mathbf{q}(t-\tau)$ (see Fig. 4). The weighting matrix has the form

$$\mathbf{D} = \begin{pmatrix} \mathbf{0} & \mathbf{0} \\ \mathbf{H} & \mathbf{0} \end{pmatrix} \tag{17}$$

Note that this case corresponds to the standard zeroth-order semi-discretization method given in [10].

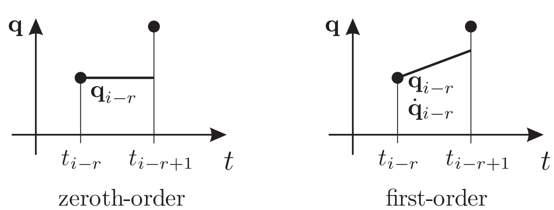

Fig. 4 Sketch of the zeroth- and the first-order one-point methods

2.1.2 First-order approximation

This method uses the discrete vector $\mathbf{q}(t_{i-r})$ and its derivative $\dot{\mathbf{q}}(t_{j-r})$ to approximate $\mathbf{q}(t-\tau)$ (see Fig. 4). It can be seen from the structure of the step matrix $\mathbf{G}$ that the derivatives of $\mathbf{q}$ are introduced to the augmented state vector only because the velocity is present in the control force. These derivatives can be used to give a better approximation for the delayed state variables, which give rise to the first-order approximation, where the delayed term is approximated as $\mathbf{q}(t-\tau) \approx \mathbf{q}(t_{i-r}) + \dot{\mathbf{q}}(t_{i-r})(t-t_{i-r})$. The corresponding weighting matrix reads

$$\mathbf{D}(t) = \begin{pmatrix} \mathbf{0} & \mathbf{0} \\ \mathbf{H} & \mathbf{H}t \end{pmatrix} \tag{18}$$

Note that this first-order approximation is different from the one presented in [10]. Here the first-order approximation of the past state is obtained using $\mathbf{q}(t_{j-r})$ and its derivative $\dot{\mathbf{q}}(t_{j-r})$, while in [10], the first-order approximation is obtained using two subsequent discrete state variables $\mathbf{q}(t_{j-r})$ and $\mathbf{q}(t_{j-r+1})$. This latter case here is called as two-point method.

2.2 *Two-point methods*

Two-point methods take the past values from two subsequent discrete time instants for the approximation of the delayed function. The approximation of equation (2) for the time interval $t \in [t_i, t_{i+1})$ can be given as

$$\dot{\mathbf{x}}(t) = \mathbf{A}\mathbf{x}(t) + \mathbf{D}_1(t)\mathbf{x}_{i-r} + \mathbf{D}_2(t)\mathbf{x}_{i-r+1} + \mathbf{C}\mathbf{x}_{i-p}, \tag{19}$$

where the weighting matrices $\mathbf{D}_1(t)$ and $\mathbf{D}_2(t)$ depend on the order of the approximation and on the weighting between the past values. Similarly to equation (4) the solution of equation (19) can be determined by the variation of constants formula. The relation between the two endpoints of the discretization step is

$$\mathbf{x}_{i+1} = \mathbf{P}\mathbf{x}_i + \mathbf{R}_1\mathbf{x}_{i-r} + \mathbf{R}_2\mathbf{x}_{i-r+1} + \mathbf{R}_C\mathbf{x}_{i-p}, \tag{20}$$

where

$$\begin{gathered} \mathbf{P} = \mathbf{e}^{\mathbf{A}h}, \quad \mathbf{R}_1 = \int_0^h \mathbf{e}^{\mathbf{A}(h-t)}\mathbf{D}_1(t)\mathrm{d}t, \\ \mathbf{R}_2 = \int_0^h \mathbf{e}^{\mathbf{A}(h-t)}\mathbf{D}_2(t)\mathrm{d}t, \quad \mathbf{R}_C = \int_0^h \mathbf{e}^{\mathbf{A}(h-t)}\mathbf{C}\mathrm{d}t. \end{gathered} \tag{21}$$

The coefficient matrices $\mathbf{G}$ for two-point methods have similar forms as the ones for the one point methods. The only difference is that one more sub-matrix appears on the right end of the top row. The location of the sub-matrix $\mathbf{R}_C$ for different discretization steps is the same, after each discrete step, this matrix jumps to the right by one, as it is shown in Fig. 5. In the next points, semi-discretization schemes of different orders are presented for the two-point method.

$$\left[\ \overbrace{\mathbf{P}\ \ \mathbf{0}\ \dots\ \mathbf{0}}^{p}\ \ \overbrace{\mathbf{R}_C\ \ \mathbf{0}\ \dots\ \mathbf{0}\ \ \mathbf{0}}^{p}\ \ \overbrace{\mathbf{0}\ \dots\ \mathbf{0}\ \ \mathbf{R}_1}^{r-2p+1}\ \ \mathbf{R}_2\ \right]$$

Fig. 5 Top row of $\mathbf{G}$ matrices for two-point methods

2.2.1 Zeroth-order approximation

This method takes the average of the state variable $\mathbf{q}(t)$ at two past time instants, namely at $\mathbf{q}(t_{i-r})$ and $\mathbf{q}(t_{i-r+1})$ to approximate $\mathbf{q}(t-\tau)$ (see Fig. 6). The weighting matrices are

$$\mathbf{D}_1 = \mathbf{D}_2 = \begin{pmatrix} \mathbf{0} & \mathbf{0} \\ \frac{1}{2}\mathbf{H} & \mathbf{0} \end{pmatrix}. \tag{22}$$

Note that this case corresponds to the improved zeroth-order semi-discretization used in [10].

2.2.2 First-order approximation

In this method, the delayed term $\mathbf{q}(t-\tau)$ is approximated as a linear function of time using the discrete values $\mathbf{q}(t_{i-r})$ and $\mathbf{q}(t_{i-r+1})$ (see Fig. 6). The weighting matrices are

$$\mathbf{D}_1(t) = \begin{pmatrix} \mathbf{0} & \mathbf{0} \\ (1-t/h)\mathbf{H} & \mathbf{0} \end{pmatrix}, \quad \mathbf{D}_2(t) = \begin{pmatrix} \mathbf{0} & \mathbf{0} \\ t/h\mathbf{H} & \mathbf{0} \end{pmatrix}. \tag{23}$$

Note that this case corresponds to the first-order semi-discretization used in [10].

2.2.3 Second-order approximation

This method approximates the state variable values between two past time instants by using not only the past values of the function but also their derivatives. Namely,

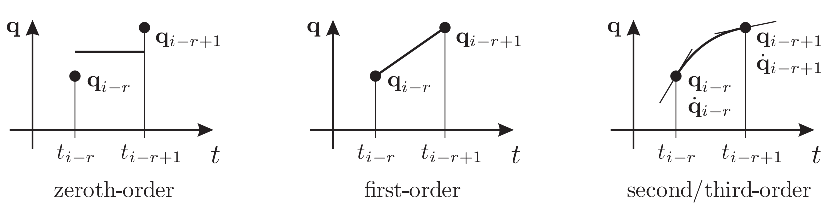

Fig. 6 Sketch of the zeroth-, the first-, the second- and the third-order two-point methods

$\mathbf{q}(t-\tau)$ is approximated by a second-order function using the values $\mathbf{q}(t_{i-r})$, $\mathbf{q}(t_{i-r+1})$ and $\dot{\mathbf{q}}(t_{j-r})$ or $\dot{\mathbf{q}}(t_{j-r+1})$ (see Fig. 6). The second order function is constructed by the linear interpolation between two first order one point approximations at time instants t_{i-r} and t_{i-r+1}. The weighting matrices read

$$\mathbf{D}_1(t) = \begin{pmatrix} \mathbf{0} & \mathbf{0} \\ (1-t/h)\mathbf{H} & t\mathbf{I} \end{pmatrix}, \quad \mathbf{D}_2(t) = \begin{pmatrix} \mathbf{0} & \mathbf{0} \\ t/h\mathbf{H} & (t-h)t/h\mathbf{H} \end{pmatrix}. \tag{24}$$

Note that this discretization concept is different from the ones presented in [10].

2.2.4 Third-order approximation

In this method, the delayed term $\mathbf{q}(t-\tau)$ is approximated by the discrete values $\mathbf{q}(t_{i-r})$, $\mathbf{q}(t_{i-r+1})$ of the state variables and its derivatives $\dot{\mathbf{q}}(t_{j-r})$ and $\dot{\mathbf{q}}(t_{j-r+1})$ (see Fig. 6). The weighting matrices are

$$\mathbf{D}_1(t) = \begin{pmatrix} \mathbf{0} & \mathbf{0} \\ \left(1-3\left(\frac{t}{h}\right)^2+2\left(\frac{t}{h}\right)^3\right)\mathbf{H} & t\left(1-2\frac{t}{h}+\left(\frac{t}{h}\right)^2\right)\mathbf{H} \end{pmatrix}, \tag{25}$$

$$\mathbf{D}_2(t) = \begin{pmatrix} \mathbf{0} & \mathbf{0} \\ \left(3\left(\frac{t}{h}\right)^2-2\left(\frac{t}{h}\right)^3\right)\mathbf{H} & t\left(-\frac{t}{h}+\left(\frac{t}{h}\right)^2\right)\mathbf{H} \end{pmatrix}. \tag{26}$$

This discretization concept is different from the ones presented in [10].

Comparison of the above methods for different period resolutions shows that the third-order two-point method provides the fastest convergence. Therefore, this method will be used for the for the forthcoming examples.

3 Example: the delayed oscillator

Consider first the delayed oscillator subjected to a digital PD controller [13]. The governing equation can be written in the form

$$\ddot{x}(t)+a_1\dot{x}(t)+a_0x(t) = b_0x(t-\tau)-Px(t_{j-1})-D\dot{x}(t_{j-1}), \quad t\in[t_j,t_{j+1}) \tag{27}$$

where $t_j = j\Delta t$ are the sampling instants for the controller, Δt is the sampling period, P is the proportional gain and D is the derivative gain. The stability chart of this DDE for $P=0$ and $D=0$ is well known in the literature (see the diagrams $P=0$ and $D=0$ in Figures 7 and 8).

The first order representation of equation (27) reads

$$\dot{\mathbf{x}}(t) = \mathbf{A}\mathbf{x}(t)+\mathbf{B}\mathbf{x}(t-\tau)+\mathbf{C}\mathbf{x}(t_{j-1}), \quad t\in[t_j,t_{j+1}), \tag{28}$$

where

$$\mathbf{x}(t) = \begin{pmatrix} x(t) \\ \dot{x}(t) \end{pmatrix}, \ \mathbf{A} = \begin{pmatrix} 0 & 1 \\ -a_0 & -a_1 \end{pmatrix}, \ \mathbf{B} = \begin{pmatrix} 0 & 0 \\ b_0 & 0 \end{pmatrix}, \ \mathbf{C} = \begin{pmatrix} 0 & 0 \\ -P & -D \end{pmatrix}. \quad (29)$$

Figures 7 and 8 present a series of stability diagrams for different (both negative and positive) proportional and derivative control gains for $\kappa = 2$ and 20. The horizontal and vertical axes are a_0 and b_0 parameters, respectively. The charts were determined by the third-order two-point semi-discretization method. Note that $\kappa = r/p = \tau/\Delta t$, which describes the ratio of the time delay τ and the sampling period Δt. The stability diagrams were obtained numerically by analyzing the eigenvalues of the transition matrix $\mathbf{\Phi}$ for a series of fixed parameters.

For large κ values, the sampling period Δt of the digital controller is much smaller than the system delay τ. In these cases, the PD controller practically results in an artificial stiffness and a damping in the system, since $a_0 x(t) + P x(t_{j-1}) \approx (a_0 + P)x(t)$ and $a_1 \dot{x}(t) + D\dot{x}(t_{j-1}) \approx (a_1 + D)\dot{x}(t)$ if $t \in [t_j, t_{j+1})$, $t_j = j\Delta t$ and $\Delta t \ll 1$. This tendency can be observed in Fig. 8 (for the case $\kappa = \tau/\Delta t = 20$): positive proportional gains result in a shift of the stability diagram to the left, while positive derivative gains increase the area of the stability domains. An interesting feature in this case is that the stabilizing effect of the positive derivative gains is stronger for negative proportional gains than for positive ones.

For smaller κ values (see Fig. 7), the connection between the control gains and the stability of the system is not so trivial. In these cases, the sampling period Δt of the digital controller and the system delay τ is commensurate, and the combination of the two kind of time delays results in intricate stability charts.

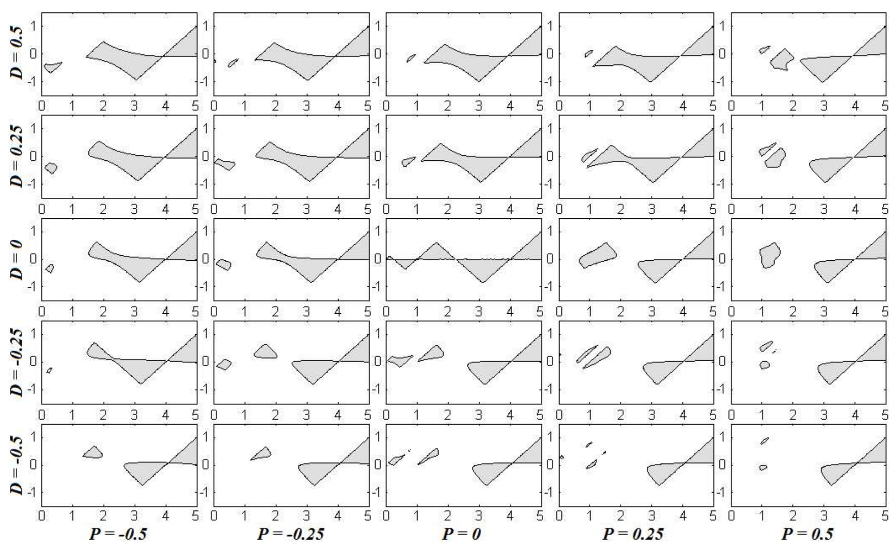

Fig. 7 Stability charts for equation (27) with κ=2, a_1=0, $\tau = 2\pi$ for delay resolution r=40

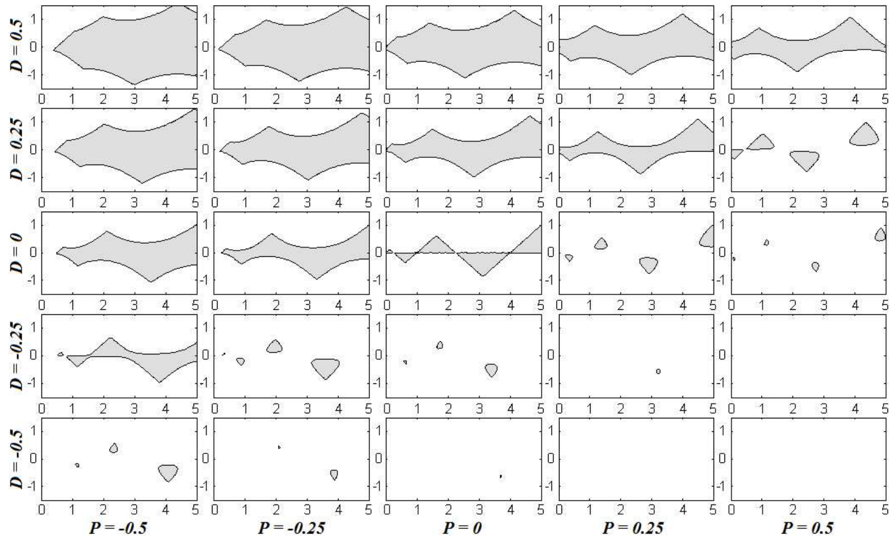

Fig. 8 Stability charts for equation (27) with κ=20, a_1=0, $\tau = 2\pi$ for delay resolution r=40

4 Example: application to turning processes

Regenerative machine tool chatter is one of the main limitations of increasing the material removal rate in machining processes [14]. There are several methods and ideas to suppress machine tool chatter, such as the vibration absorber [23], impedance modulation [20], spindle speed variation [21,30] or active control [8,15]. Here, the single degree-of-freedom model of a turning process subjected to a digital PD controller is analyzed. The mechanical model with modal mass m, stiffness k and damping c can be seen in Fig. 9. The linearized governing equation forms as

$$\ddot{\xi}(t) + 2\zeta\omega_n\dot{\xi}(t) + (H + \omega_n^2)\xi(t) = H\xi(t-\tau) - k_\mathrm{p}\xi(t_{j-1}) - k_\mathrm{d}\dot{\xi}(t_{j-1})\ , \quad (30)$$

where $t \in [t_j, t_{j+1})$, $\xi(t) = x(t) - x_0$ is the displacement around the trivial equilibrium point x_0, $\omega_n = \sqrt{k/m}$ is the undamped natural frequency of the tool, $\zeta = c/(2m\omega_n)$ is the damping ratio of the tool , H is the specific cutting-force coefficient, $Q/m = k_\mathrm{p}\xi(t_{j-1}) + k_\mathrm{d}\dot{\xi}(t_{j-1})$ is the specific control force and k_p and k_d are the proportional and derivative control gains [13]. Equation (30) has the same form as (27), hence the stability chart for equation (30) can be analysed by semi-discretization in the same way as for (27). Fig. 10 presents a series of stability diagrams for different (both negative and positive) proportional and derivative control gains for $\kappa = \tau/\Delta t = 20$. The horizontal axis is the dimensionless spindle speed $\Omega/(60f_n)$, where the spindle speed is $\Omega = 60/\tau$ and the natural frequency of the tool is $f_n = \omega_n/(2\pi)$. The vertical axis is the dimensionless specific cutting-force coefficient H/ω_n^2. In this diagram the exact stability boundaries of the turning

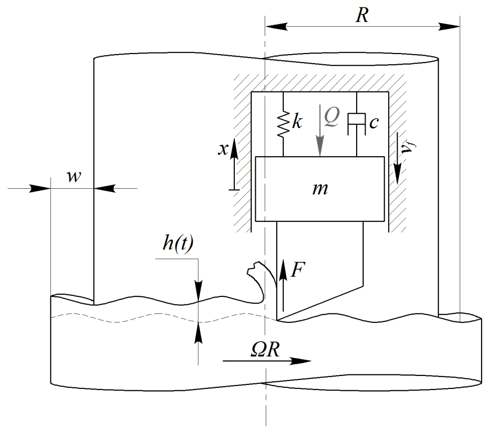

Fig. 9 Sketch of the mechanical model

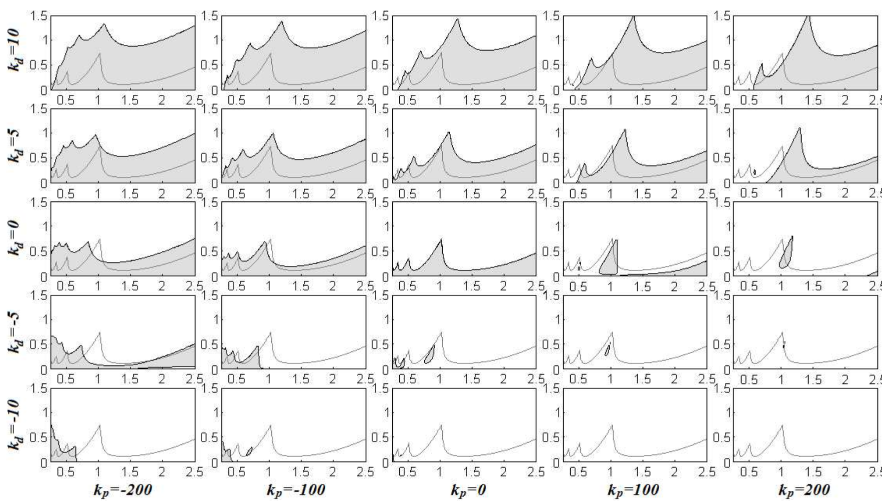

Fig. 10 Stability charts for turning processes with different control parameters for κ=20, r=20 and ζ=0.05

process without any control are presented by gray line. The stability diagrams were obtained in the same way as for equation (27). It can be seen that the most important control parameter is the derivative gain k_{d}. Positive derivative gains result in a kind of artificial damping parameter in the system. The effect of the proportional gain k_{p} on the stability is not so significant. Similarly to the delayed oscillator, the stabilizing effect of the positive derivative gains is stronger for negative proportional gains.

5 Conclusions

Dynamical systems with continuous point delay terms in the form $x(t-\tau)$ and discrete delayed terms in the form $x(t_{j-1})$, $t \in [t_j, t_{j+1})$, $t_j = j\Delta t$ were analyzed using the semi-discretization method. These systems typically arise if a delayed system is subjected to a digital feedback controller. Different approaches were presented based on the number of the discretization points and based on the order of the approximation of the delayed term. Stability diagrams were determined for the delayed oscillator with digital controller and, as a practical application, stabilization of turning processes with digital feedback controller was analyzed.

The results related to the delayed oscillator are shown in Figures 7 and 8. The results for the stabilization of the turning process is presented in Fig. 10. The main conclusion is that if the feedback controller is fast enough compared to the time delay in the uncontrolled system, then, since $x(t_{j-1}) \approx x(t)$ and $\dot{x}(t_{j-1}) \approx \dot{x}(t)$ on $t \in [t_j, t_{j+1})$, $t_j = j\Delta t$, positive proportional and derivative gains act as a kind of artificial stiffness and damping in the system. Therefore if $\kappa \gg 1$ then, considering stability, an analogue PD control approximates well the digital PD control. In this case, it was observed that the stabilizing effect of the positive derivative gains is stronger for negative proportional gains. If the sampling period Δt of the feedback controller is commensurate to the system delay τ, then the combination of the two kind of time delays result in an intricate stability picture.

In the equations analyzed in this paper, two types of delays were present: the continuous delay $x(t-\tau)$ and the discrete delay $x(t_{j-1})$. While the continuous delay attributes an infinite dimensional nature to the system, the discrete delay presents a kind of intermittence or discontinuity in the system. This combination of time delays may also be important in human balancing models with reflex delay, where the human motor control is often modeled as a system with discontinuous feedback [6,16,27].

Acknowledgements This work was supported by the Hungarian National Science Foundation under grant OTKAK105433. The first author was supported by the Rostoczy Foundation Scholarship Program.

References

1. Bachrathy D, Stepan G, Turi J (2011) State dependent regenerative effect in milling processes. J Comput Nonlin Dyn–T ASME, 6:041002.
2. Butcher EA, Ma H, Bueler E, Averina V, Szabó Zs (2004) Stability of time-periodic delay-differential equations via Chebyshev polynomials. Int J Numer Mech Eng 59:895–922.
3. Ding Y, Zhu LM, Zhang XJ, Ding H (2010) A full-discretization method for prediction of milling stability. Int J Mach Tool Manu 50:502–509.
4. Dombovari Z, Altintas Y, Stepan G (2010) The effect of serration on mechanics and stability of milling cutters. Int J Mach Tool Manu 50:511–520.
5. Farkas M (1994) Periodic motions. Springer-Verlag, New York.

6. Gawthrop P, Loram I, Lakie M, Gollee H (2011). Intermittent control: a computational theory of human control. Biol Cybern 104:31–51
7. Hale JK (1977). Theory of functional differential equations. Springer-Verlag, New York.
8. Hu Q, Krawcewicz W, Turi J (2012) Stabilization in a state-dependent model of turning processes, SIAM J Appl Math 72:1-24.
9. Insperger T, Stepan G (2002). Semi-discretization method for delayed systems. Int J Numer Meth Eng 55:503–518.
10. Insperger T, Stepan G (2011). Semi-Discretization for Time-Delay Systems. Springer, New York.
11. Khasawneh FA, Mann BP (2011). A spectral element approach for the stability of delay systems. Int J Numer Meth Eng 87:566–592.
12. Lampe BP, Rosenwasser EN (2011) Stability investigation for linear periodic time-delayed systems using Fredholm theory. Automat Rem Contr 72(1):38–60.
13. Lehotzky D, Insperger T (2012) Stability of delayed oscillators subjected to digital PD control. 10th IFAC Workshop on Time Delay Systems, Boston, USA. IFAC-PapersOnline.
14. Mancisidor I, Zatarain M, Munoa J, Dombovari Z (2011) Fixed boundaries receptance coupling substructure analysis for tool point dynamics prediction. Adv Mat Res 223:622-631
15. Munoa J, Mancisidor I, Loix N, Uriarte LG, Barcena R, Zatarain M (2013) Chatter suppression in ram type travelling column milling machines using a biaxial inertial actuator. CIRP Ann–Manuf Techn, in press.
16. Milton J, Townsend JL, King MA, Ohira T (2009). Balancing with positive feedback: the case for discontinuous control. Philos T R Soc A 367:1181–1193.
17. Orosz G, Stepan G (2006) Subcritical Hopf bifurcations in a car-following model with reaction-time delay. P Roy Soc A–Math Phy 462:2643–2670.
18. Pohlmann KC (2000). Principles of Digital Audio. McGraw-Hill, New York.
19. Quo Q, Sun Y, Jiang Y (2012) On the accurate calculation of milling stability limits using third-order full-discretization method. Int J Mach Tool Manu 62:61–66.
20. Segalman DJ, Butcher EA (2000). Suppression of regenerative chatter via impendance modulation. J Vib Control 6:243–256.
21. Seguy S, Insperger T, Arnaud L, Dessein G, Peigne G (2010) On the stability of high-speed milling with spindle speed variation. Int J Adv Manuf Tech 48:883–895.
22. Sieber J, Szalai R (2011) Characteristic matrices for linear periodic delay differential equations. SIAM J Appl Dyn Sys 10(1):129–147.
23. Sims ND (2000). Vibration absorbers for chatter suppression: a new analytical tuning methodology. J Sound Vib 301:592–607.
24. Stepan G (2001). Vibrations of machines subjected to digital force control. Int J Solids Struct 38:2149–2159.
25. Sun JQ (2009) A method of continuous time approximation of delayed dynamical systems. Commun Nonlinear Sci 14:998–1007.
26. Sun J-Q, Song B (2009) Control studies of time-delayed dynamical systems with the method of continuous time approximation. Commun Nonlinear Sci Numer Simulat 14:3933-3944.
27. Suzuki Y, Nomura T, Casadio M, Morasso P (2012) Intermittent control with ankle, hip, and mixed strategies during quiet standing: A theoretical proposal based on a double inverted pendulum model. J Theor Biol 310:55–79.
28. Szalai R, Stepan G, Hogan SJ (2006) Continuation of bifurcations in periodic delay-differential equations using characteristic matrices. SIAM J Sci Comput 28:1301–1317.
29. Takacs D, Orosz G, Stepan G (2009) Delay effects in shimmy dynamics of wheels with stretched-string like tyres. Eur J Mech A-Solid 28:516–525.
30. Zatarain M, Bediaga I, Munoa J, Lizarralde R (2008) Stability of milling processes with continuous spindle speed variation: Analysis in the frequency and time domains, and experimental correlation. CIRP Ann–Manuf Techn 57:379–384.